Friction **9**(4): 747–757 (2021)
https://doi.org/10.1007/s40544-020-0369-0
ISSN 2223-7690
CN 10-1237/TH
RESEARCH ARTICLE

MoS_2 nanoparticles grown on carbon nanomaterials for lubricating oil additives

Kuiliang GONG[1,2], Wenjing LOU[1,3], Gaiqing ZHAO[1,3], Xinhu WU[1,3,*], Xiaobo WANG[1,3,*]

[1] *State Key Laboratory of Solid Lubrication, Lanzhou Institute of Chemical Physics, Chinese Academy of Sciences, Lanzhou 730000, China*

[2] *University of Chinese Academy of Sciences, Beijing 100049, China*

[3] *Qingdao Center of Resource Chemistry & New Materials, Qingdao 266000, China*

Received: 05 September 2019 / Revised: 25 December 2019 / Accepted: 08 February 2020

Abstract: In this study, the nanocomposites of MoS_2 nanoparticles (NPs) grown on carbon nanotubes (MoS_2@CNT), graphene (MoS_2@Gr), and fullerene C60 (MoS_2@C60) were synthesized, characterized, and evaluated for potential use as lubricant additives. By using the benefit of the synergistic effect between MoS_2 and carbon nanomaterials (CNMs), these nanocomposites can be well dispersed in polyalkylene glycol (PAG) base oil and show superior stability compared with pure MoS_2 NPs. Moreover, the dispersions of MoS_2@CNT, MoS_2@Gr, and MoS_2@C60 added in PAG have noticeably improved friction reducing and antiwear (AW) behaviors at elevated temperature for comparison with that of PAG and PAG containing CNT, Gr, C60, and MoS_2 NPs, respectively. The enhanced lubricating properties of these nanocomposites were also elucidated by exploring the tribofilm formed on the disc.

Keywords: MoS_2 nanoparticle; carbon nanomaterial; nanocomposite; antifriction and antiwear additive

1 Introduction

In several modern industrial processes, machines and devices with lubricated moving parts operate at elevated temperatures. In particular, the working temperatures of lubricating oils used in the field of aviation, metallurgy, and construction material industry often exceed 200 °C [1−3]. These applications require lubricating oil with high thermal stability. High-temperature (HT) lubricating oils are usually composed of base fluids and lubricant additives. Although many synthetic base oils such as synthetic esters, polyalkylene glycol (PAG), and perfluoropolyethers (PFPE) have been developed [4−6], only a few HT lubricant additives, especially for improving the friction reduction and antiwear (AW) properties of base oils, are commercially available. For instance, tricresyl phosphate (TCP) and zinc dialkyl dithiophosphates (ZDDP), which are the traditional organic additives having excellent friction reducing and AW properties, are widely used in various applications. However, the intensive use of these additives may cause toxicity and pollution issues [7−9]. Another issue associated with the use of these additives is their fast thermal degradation accompanied with a loss of their tribological behavior under HT conditions [9]. Therefore, there is an urgent need for research on HT lubricant additives.

Extensive research has been published on the use of MoS_2 nanoparticles (NPs) as lubricating oil additives owing to their attractive characteristics [10−13], such as high chemical stability, exceptional lubricating properties, and low toxicity [9]. The MoS_2 NPs must be dispersed in base oils with long term stabilities for realizing the friction reduction and AW behavior. Previous reports have indicated that carbon nanomaterials (CNMs) could improve the oil dispersibility of MoS_2 NPs and prevent their oxidation during rubbing [14−16]. For example, Xu et al. [14] investigated the

* Corresponding authors: Xinhu WU, E-mail: wuxh@licp.cas.cn; Xiaobo WANG, E-mail: wangxb@licp.cas.cn

tribological performances of graphene, MoS_2, and graphene/MoS_2 blends dispersed in esterified bio-oil (EBO), and the results showed that graphene/MoS_2 hybrids exhibited superior friction and AW properties as compared with the addition of graphene and MoS_2 in EBO, which could be primarily attributed to the synergistic effect between graphene and MoS_2. We also fabricated the nanocomposites of MoS_2/graphene by the decomposition of MoS_3 on graphene at high temperature (800 °C), and evaluated their tribological behavior in PAG base oil [15]. This report demonstrated that the nanocomposites of MoS_2/graphene have better dispersibility in the base oil and could significantly improve the friction reduction and AW properties of PAG with respect to graphene, MoS_2, and the mixture of graphene with MoS_2 at elevated temperatures. For the in-depth study of MoS_2 with CNMs as oil additives, the preparation method for MoS_2/graphene nanocomposites without involving the use of sophisticated techniques needs to be explored. There is no report in the literature that investigates the dispersion stability and tribological performances of MoS_2 deposited on CNT and C60, as lubricating oil additives.

In this study, we synthesized MoS_2 nanoparticles grown on carbon nanotubes (MoS_2@CNT), graphene (MoS_2@Gr), and fullerene C60 (MoS_2@C60) by using a simple solvothermal method [17]. The structures of these nanocomposites are characterized by various techniques, such as field emission scanning electron microscope (FE-SEM), transmission electron microscopy (TEM) and high-resolution TEM (HRTEM), X-ray diffraction (XRD), Raman spectra, and X-ray photoelectron spectroscopy (XPS) spectra. The oil suspendability of MoS_2@CNT, MoS_2@Gr, and MoS_2@C60 in PAG is evaluated. The tribological measurements for these nanocomposites that are added in PAG base oil are carried out on an optimal SRV-V oscillating friction and wear tester. The corresponding worn surfaces of steel discs are characterized by scanning electron microscopy coupled with energy dispersive X-ray analysis (SEM-EDX) and XPS to explore the friction reduction and AW mechanism of these nanocomposites.

2 Experimental

2.1 Materials

CNMs including multiwalled CNT (8 nm × (0.5–2 μm)); diameter × length, purity ≥ 95%), ultra-thin graphene ((0.5–5 μm) × (0.8–1.2 nm); width × thickness), and C60 (purity ≥ 99.5%) were purchased from Nanjing XFNANO Materials Tech Co., Ltd. The ammonium thiomolybdate ($(NH_4)_2MoS_4$, purity ≥ 99.97%) was purchased from J&K Scientific Ltd. The hydrazine hydrate ($N_2H_4{\cdot}H_2O$, purity ≥ 85%) and N, N-dimethylformamide (DMF) were purchased from Sinopharm Chemical Reagent Co., Ltd. The deionized (DI) water was prepared by the RO-DI Laboratory water purification system. The PAG base oil was obtained from HENUVAR Chemical Corporation, and its physical and chemical properties have been reported previously [18]. All reagents and solvents were used, as received without any further purification.

2.2 Preparation

The nanocomposites of MoS_2@CNT, MoS_2@Gr, and MoS_2@C60 were prepared by the use of a simple solvothermal method with some modifications as reported by Li et al. [17]. For the preparation of MoS_2@CNT, CNT (20 mg) was sonicated with $(NH_4)_2MoS_4$ (44 mg) in DMF (20 ml) for 30 min; subsequently, $N_2H_4{\cdot}H_2O$ (0.2 ml) was added to the mixture. After ultrasonication for 30 min, the reaction solution was transferred to a 100 mL poly(tetrafluoroethlene) (Teflon) autoclave, and the autoclave was heated in an oven at 200 °C for 10 h. After being naturally cooled to the ambient temperature, the product was filtered through a 0.22 μm microporous membrane, and washed with DI water and ethanol at least 5 times, respectively. Finally, the product was dried at 60 °C in a vacuum for 12 h. The preparation method for MoS_2@Gr and MoS_2@C60 was the same as described above. For the purpose of comparison, the pure MoS_2 NPs were produced by using the same method, but without adding any CNMs (CNT, Gr, and C60).

Zhao et al. [19] have demonstrated that the base oil added with graphene and MoS_2 exhibited better tribological properties when the NPs content was 1 wt%; therefore, 1 wt% content of MoS_2@CNT, MoS_2@Gr, and MoS_2@C60 were added in PAG base oil and thoroughly mixed through ultrasonication for 30 min. For the purpose of comparison, PAG containing 1 wt% CNT, 1 wt% Gr, 1 wt% C60, and 1 wt% MoS_2 were prepared by using the same method.

2.3 Characterization techniques

The FE-SEM was performed by using a Hitachi S-4800 SEM at an accelerating voltage of 10 kV. The TEM and HRTEM images were performed on a FEI TECNAI F30 TEM operating with 200 kV accelerating voltage. The XRD was carried out on a Bruker D8 ADVANCE. The Raman spectra of these nanocomposites were recorded on Thermo Fisher DXR Raman microscope with a laser excitation wavelength of 532 nm. The XPS spectra were collected on a PHI-5702 multifunctional XPS device, using Al Kα radiation as the excitation source and the binding energy of contaminated carbon (C 1s, 284.6 eV) as a reference.

2.4 Tribological characterization

The friction reduction and AW properties of these nanoparticles were evaluated by an optimal-SRV-V reciprocation friction tester with a ball-on-disc configuration. The upper ball (Ø 10 mm, AISI 52100 steel, hardness of 57–60 HRC) runs against the stationary lower steel discs (Ø 24 mm × 7.9 mm, AISI 52100 steel, hardness of 58–60 HRC) for a duration of 30 min at a frequency of 25 Hz and amplitude of 1 mm. The friction test was repeated three times for each sample to check the reproducibility of the measurements. The coefficient of friction (COF) was recorded automatically by a computer connected to the SRV tester. The wear losses of the lower discs were measured using a MicroXAM-3D surface mapping microscope profilometer.

3 Results and discussion

3.1 Characterization of MoS_2@CNT, MoS_2@Gr, and MoS_2@C60

The FE-SEM and TEM images of MoS_2@CNT, MoS_2@Gr, and MoS_2@C60 nanocomposites are presented in Fig. 1. The MoS_2 NPs are homogeneously blended with CNT, Gr, and C60 (Figs. 1(a)–1(c)), and the particles of MoS_2 on graphene are ranging in size from 50–100 nm with a few particles larger than 100 nm, while the particle size of MoS_2 on CNT and C60 could not be observed clearly from the SEM image. Meanwhile, the microstructure of MoS_2@C60 is different from that of MoS_2@CNT and MoS_2@Gr (Fig. 1(c)), and the aggregated MoS_2 NPs with larger particle size in MoS_2@C60 nanocomposites could be observed. For the purpose of comparison, the image of pure C60 with particle size ranging from 50 to 150 nm is inset in Fig. 1(c). The TEM images display that the MoS_2 NPs are grown on the surface of CNT and Gr (Figs. 1(d) and 1(e)), and these figures show that the particle sizes and

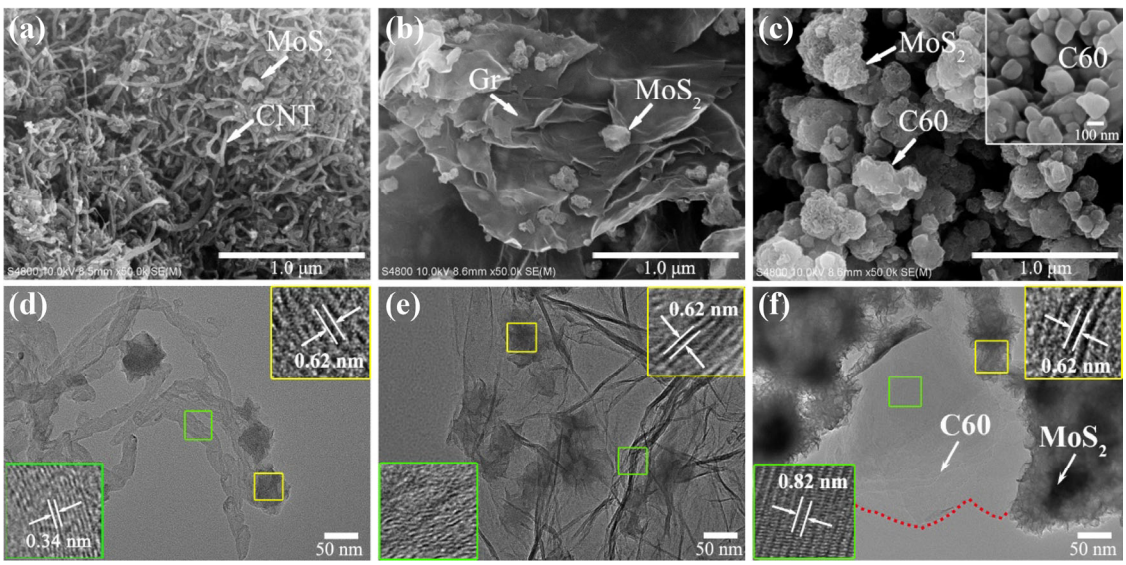

Fig. 1 Electron microscopy characterizations of MoS_2@CNMs. FE-SEM images of (a) MoS_2@CNT, (b) MoS_2@Gr, and (c) MoS_2@C60. Inset in (c) is the SEM image of pure C60. TEM images of (d) MoS_2@CNT, (e) MoS_2@Gr, and (f) MoS_2@C60. Insets in (d–f) show the magnified images of some exposed edges of MoS_2 nanosheets (zoomed from the yellow contour) and the lattice spacing of CNT (zoomed from the green contour).

morphology of MoS_2 NPs on CNT and Gr are similar to each other, with a median particle size of approximately 80 nm. However, in the nanocomposite of MoS_2@C60, the MoS_2 NPs are aggregated with particle size more than 100 nm, which are not uniformly distributed on the surface of C60 (Fig. 1(f)). Moreover, the insets in Figs. 1(d)–1(f) revealed the HRTEM image for a typical lamellar structure of MoS_2 with an interlayer spacing of 0.62 nm (the areas designated by yellow squares in Figs. 1(d)–1(f)) [20]. Apart from these, the inset in Figs. 1(d) and 1(f) also show a lattice spacing of 0.35 and 0.87 nm (zoomed from the green squares in Figs. 1(d) and 1(f)), corresponding to the (002) face of CNT [21] and the (111) lattice plane of C60 [22], respectively. The amorphous structure of Gr is also inset in Fig. 1(e) (zoomed from the green square in Fig. 1(e)). These results confirmed the formation of MoS_2@CNT, MoS_2@Gr, and MoS_2@C60.

The physical structures of MoS_2@CNT, MoS_2@Gr, and MoS_2@C60 are characterized by XRD and Raman spectra. As shown in Fig. 2(a), a weak peak at 2θ = 23.8° on the spectrum of MoS_2@C60 is assigned to the characteristic graphitic (002) of C60. The disappearance of the characteristic peak at 2θ = 23.8° for MoS_2@CNT and MoS_2@Gr might be caused by the factor that MoS_2 NPs covered the surfaces of CNT and Gr and weakened the XRD signals. The XRD spectra of MoS_2@CNT, MoS_2@Gr, and MoS_2@C60 show a very strong diffraction peak at 2θ = 14.6°, and two weak peaks at 2θ = 39.8° and 49.6°, which corresponded to (002), (103), and (105) faces of MoS_2, respectively [23, 24]. The spectra of MoS_2@CNT and MoS_2@Gr also displayed a diffraction peak at 2θ = 32.6°, corresponding to (100) face of MoS_2, while this characteristic peak is not observed on the spectrum of MoS_2@C60. On the Raman spectroscopy of MoS_2@CNT, MoS_2@Gr, and MoS_2@C60 (Fig. 2(b)), the characteristic peaks of MoS_2 at 375 and 402 cm^{-1}, and the D, G, and 2D bonds of CNT and Gr are clearly revealed. Additionally, four peaks at 268, 491, 1,456, and 1,570 cm^{-1} are typical for C60 [25]. These results indicated that the nanocomposites of MoS_2@CNT, MoS_2@Gr, and MoS_2@C60 have been successfully prepared.

The chemical compositions and the atomic valence states of MoS_2@CNT, MoS_2@Gr, and MoS_2@C60 nanocomposites are analyzed by using XPS. The survey spectra and the atomic percentage of these nanocomposites are shown in Fig. 3(a) and Table 1. It is found that the content of MoS_2 NPs in MoS_2@CNT, MoS_2@Gr, and MoS_2@C60 is 9.97 wt%, 10.2 wt%, and 10.0 wt%, respectively. Moreover, the C 1s XPS spectrum of MoS_2@CNT contained three different peaks located at 284.6, 286.5, and 288.4 eV (Fig. 3(b)), which are assigned to C=C/C–C, C–O, and COOH groups [20], respectively. For the nanocomposites of MoS_2@Gr and MoS_2@C60, the C 1s XPS spectra are similar to each other with a binding energy at 284.6 eV (C=C/C–C) and displayed a small peak at 286.5 eV (C–O). These results indicated that MoS_2@CNT contained a small amount of COOH and OH groups, which might be derived from the precursor of CNT, not formed during the solvothermal process. The Mo 3d XPS spectra of MoS_2@CNT, MoS_2@Gr, and MoS_2@C60 are also similar to each other (Fig. 3(c)), and the peaks centered at 226.2, 229.1, and 232.3 eV are attributed to S 2s, Mo^{4+} $3d_{5/2}$, and Mo^{4+} $3d_{3/2}$, respectively, which are characteristic of MoS_2 [20]. Meanwhile, the S 2p spectra of MoS_2@CNT and

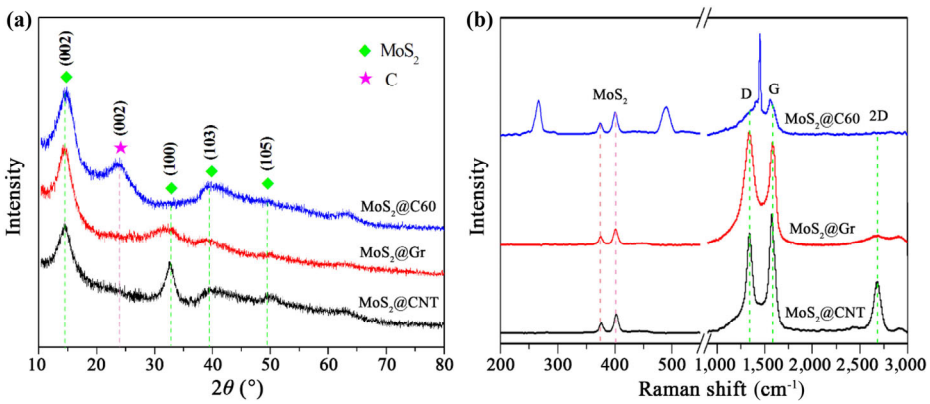

Fig. 2 (a) XRD and (b) Raman spectra of MoS_2@CNT, MoS_2@Gr, and MoS_2@C60 nanocomposites.

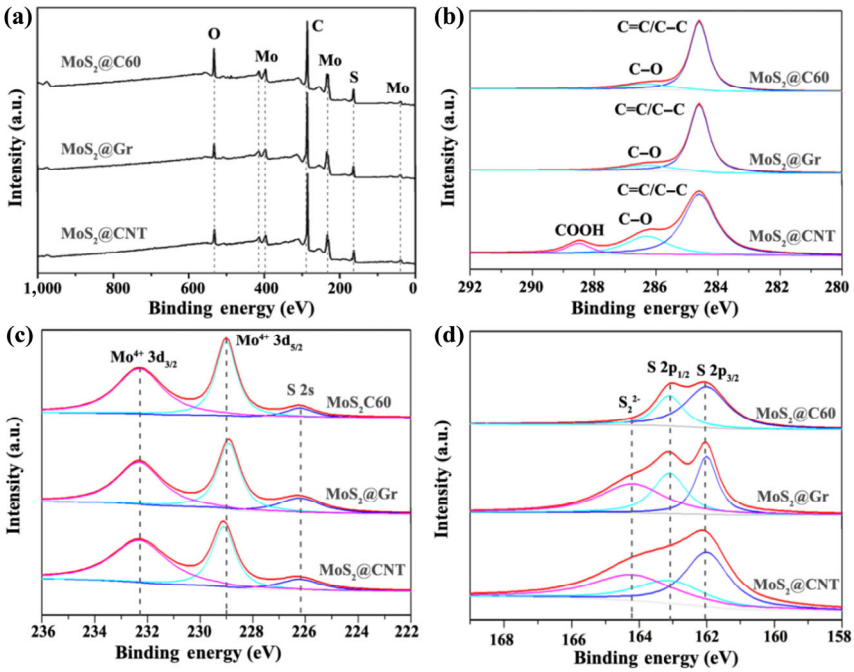

Fig. 3 XPS spectra of MoS_2@CNT, MoS_2@Gr, and MoS_2@C60 nanocomposites. (a) Survey spectra, high resolution XPS spectra of (b) C 1s, (c) Mo 3d, and (d) S 2p.

Table 1 Atomic percentage of MoS_2@CNT, MoS_2@Gr, and MoS_2@C60 nanocomposites.

Sample	Element			
	C (wt%)	O (wt%)	Mo (wt%)	S (wt%)
MoS_2@CNT	78.82	6.49	5.87	8.82
MoS_2@Gr	77.28	7.12	6.12	9.48
MoS_2@C60	71.69	12.22	6.0	10.09

MoS_2@Gr showed three peaks at 162.0, 163.1, and 164.2 eV (Fig. 3(d)), corresponding to S $2p_{3/2}$, S $2p_{1/2}$, and S_2^{2-} [26], respectively. The spectrum of MoS_2@C60 displayed two peaks at 162.0 eV (S 2p3/2) and 163.1 eV (S $2p_{1/2}$). The results mentioned above further demonstrated that the nanocomposites of MoS_2@CNT, MoS_2@Gr, and MoS_2@C60 are synthesized by using the solvothermal method.

To examine the dispersibility of MoS_2@CNT, MoS_2@Gr, and MoS_2@C60 in PAG base oil, Fig. 4 shows the base oil containing different additives photographed after 1 day (Fig. 4(a)) and two weeks (Fig. 4(b)). It can be observed that 1 wt% Gr, 1 wt% C60, 1 wt% MoS_2@CNT, 1 wt% MoS_2@Gr, and 1 wt% MoS_2@C60 dispersed in PAG are stable and resist sedimentation for 2 weeks after preparation, whereas the addition of 1 wt% MoS_2 NPs in PAG failed to disperse, in which the MoS_2 NPs aggregation is severe with a large amount of bottom sediment. This result indicated that the combination of CNT, Gr, and C60 with MoS_2 can dramatically improve the oil dispersibility of MoS_2 NPs.

3.2 Tribological properties

The friction reduction and AW properties of PAG added with 1 wt% MoS_2@CNT, 1 wt% MoS_2@Gr, and

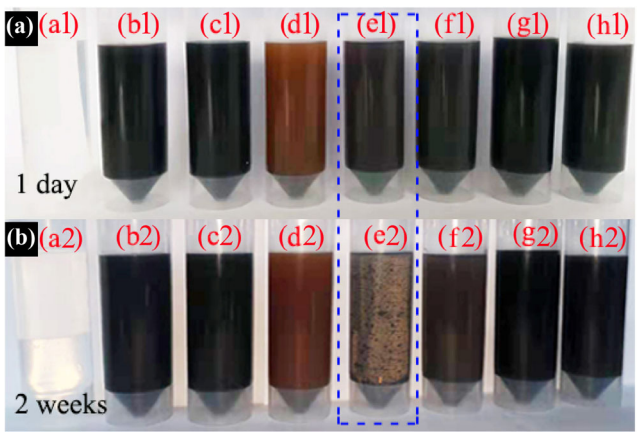

Fig. 4 Digital images of (a1, a2) PAG base oil and PAG with (b1, b2) 1 wt% CNT, (c1, c2) 1 wt% Gr, (d1, d2) 1 wt% C60, (e1, e2) 1 wt% MoS_2 NPs, (f1, f2) 1 wt% MoS_2@CNT, (g1, g2) 1 wt% MoS_2@Gr, and (h1, h2) 1 wt% MoS_2@C60 after keeping for (a) 1 day and (b) 2 weeks.

1 wt% MoS_2@C60 are investigated by SRV at 100 °C for comparison with PAG containing 1 wt% CNT, 1 wt% Gr, 1 wt% C60, and 1 wt% MoS_2 NPs. As shown in Fig. 5(a), the friction curve of PAG base oil is low and stable (COF, 0.072) for the initial 180 s, then the COF suddenly increased to 0.129, which lasted for tens of seconds, and afterwards decreased and stabilized at a value of around 0.12. The friction trend of 1 wt% CNT, 1 wt% Gr, 1 wt% C60, and 1 wt% MoS_2 added in PAG showed a similar sequence to that of the base oil, but the addition of these additives exhibited a longer initial time with slightly larger friction coefficient (COF > 0.079), which can be interpreted as follows: the addition of these additives might generate a boundary lubrication film at the initial phases; subsequently, the film wears out and is unable to form rapidly because of low absorption strength or low concentration due to the aggregation of additive at HT condition. However, the addition of 1 wt% MoS_2@CNT and 1 wt% MoS_2@Gr in PAG base oil displayed low and stable friction curves (COF, 0.082–0.091) throughout the friction process. The excellent friction reduction property might be attributed to the fact that CNT and Gr could improve the retention of MoS_2 NPs on the worn surfaces and prevent MoS_2 oxidation during the sliding process, resulting in the formation of thick protection films on the rubbing surfaces. However, the COF of PAG added with 1 wt% MoS_2@C60 slowly increased with the increase in sliding time, and finally stabilized at the value comparable to that of PAG added with MoS_2 NPs. The plausible reason being that C60 with a small surface area could not prevent MoS_2 NPs oxidation during rubbing [14], and the aggregation of MoS_2 NPs in MoS_2@C60 might weaken the improvement of the tribological properties. Furthermore, the corresponding wear losses of the steel discs lubricated by PAG having these nano-additives are shown in Fig. 5(b). It can be clearly observed that the addition of 1 wt% MoS_2@CNT, 1 wt% MoS_2@Gr, and 1 wt% MoS_2@C60 could reduce the wear losses by about 98%, 98%, and 96% with respect to the base oil, respectively. The AW performances of these nanocomposites are also dramatically better than those of CNT, Gr, C60, and MoS_2, indicating excellent AW properties of these nanocomposites at an elevated temperature.

The morphologies of wear surfaces lubricated by PAG and PAG with different additives at 100 N and 100 °C are further investigated by using SEM and 3D surface mapping profilometer. It can be clearly observed that the wear scar, which is lubricated by PAG base oil is considerably broad and deep (Figs. 6(a) and 6(a')), indicating that severe wear occurred on the steel surfaces. The width and length of the wear scars lubricated by 1 wt% CNT, 1 wt% Gr, and 1 wt% C60 are essentially the same as those lubricated by PAG (Figs. 6(b, b')–6(d, d')), indicating that the addition of CNT, Gr, and C60 could not effectively improve the AW behavior of the base oil at an elevated temperature. However, the wear scar width is smaller for the steel disc lubricated with 1 wt% MoS_2 (Figs. 6(e) and 6(e')), which shows that MoS_2 NPs has certain AW properties. In contrast, when 1 wt% MoS_2@CNT, 1 wt% MoS_2@Gr, and 1 wt% MoS_2@C60 are added in PAG base oil, the

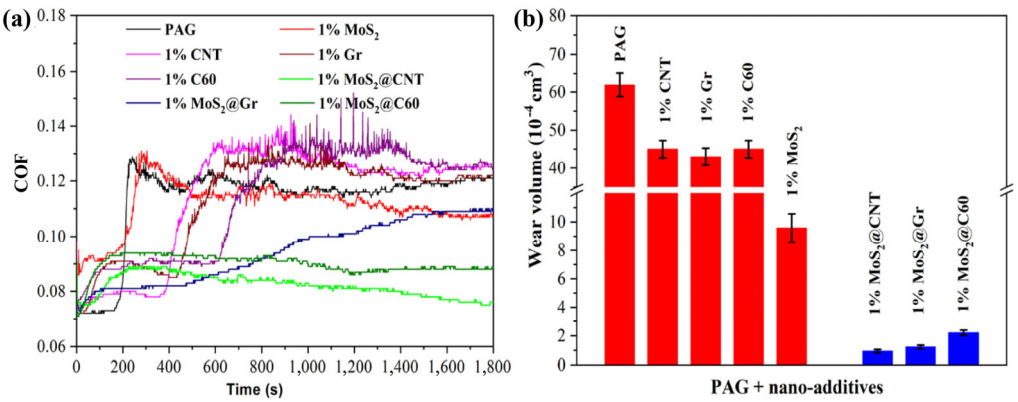

Fig. 5 (a) COF and (b) wear volumes of steel discs lubricated by PAG base oil and PAG additized with 1 wt% CNT, 1 wt% Gr, 1 wt% C60, 1 wt% MoS_2, 1 wt% MoS_2@CNT, 1 wt% MoS_2@Gr, and 1 wt% MoS_2@C60 at 100 °C (SRV conditions: load, 100 N; stroke, 1 mm; frequency, 25 Hz; duration, 30 min).

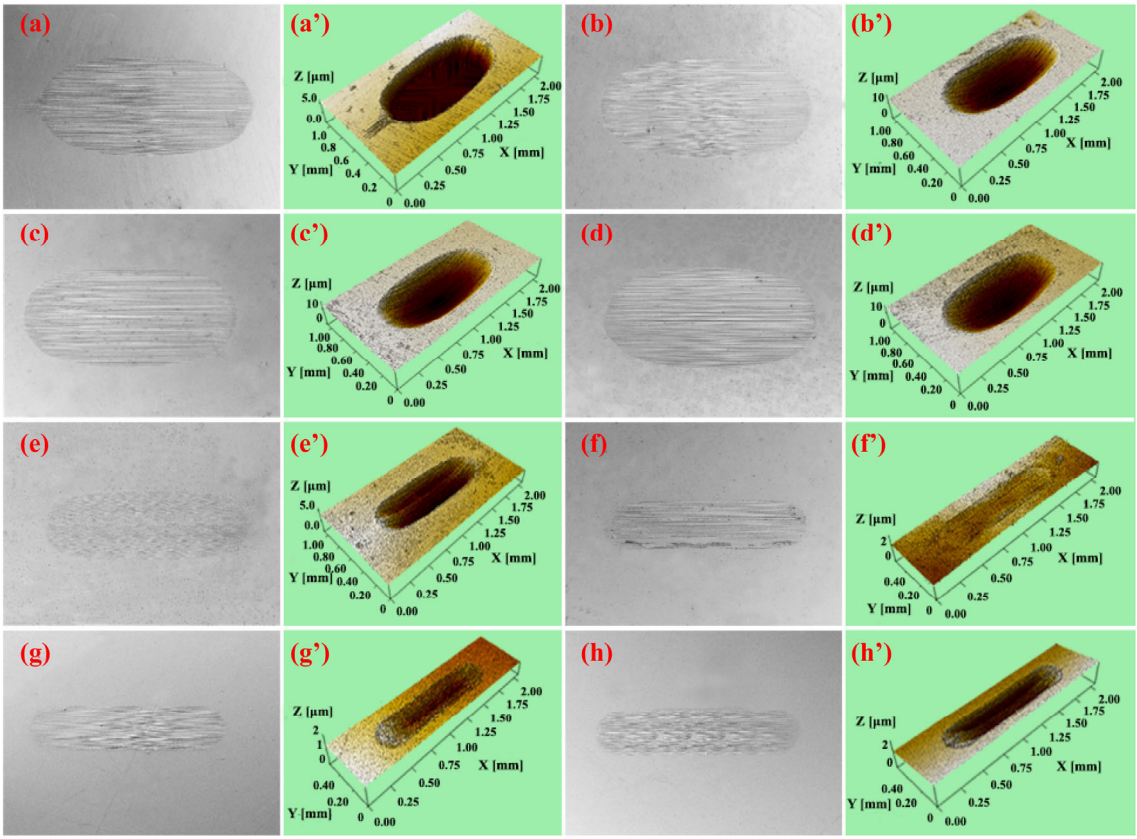

Fig. 6 (a–h) SEM and (a'–h') 3D optical microscopic images of the wear scars lubricated by (a, a') PAG base oil, and PAG additized with (b, b') 1 wt% CNT, (c, c') 1 wt% Gr, (d, d') 1 wt% C60, (e, e') 1 wt% MoS_2, (f, f') 1 wt% MoS_2@CNT, (g, g') 1 wt% MoS_2@Gr, and (h, h') 1 wt% MoS_2@C60 at 100 °C (SRV conditions: load, 100 N; stroke, 1 mm; frequency, 25 Hz; duration, 30 min).

wear scars become narrow and shallow (Figs. 6(f, f')–6(h, h')), showing that mild wear occurred on the steel discs. This is consistent with the wear volume result in Fig. 5(b).

The friction reduction and AW properties of 1 wt% MoS_2@CNT, 1 wt% MoS_2@Gr, and 1 wt% MoS_2@C60 are further investigated under various temperatures and loads. Figure 7(a) shows the evolution of friction curves with time during a temperature ramp test from 50 to 200 °C for PAG added with these nanocomposites at a constant load of 100 N. It is observed that PAG containing 1 wt% MoS_2@CNT, 1 wt% MoS_2@Gr, and 1 wt% MoS_2@C60 could effectively reduce the COF of the base oil when the temperature below 125 °C. Meanwhile, Fig. 7(b) displays the load ramp test from 50 to 300 N at 100 °C for the nanocomposite additives. It is observed that the maximum load carrying capacity of PAG can be improved from 100 to 250, 200, and 150 N by the addition of MoS_2@CNT, MoS_2@Gr, and MoS_2@C60, respectively. The results mentioned above demonstrated that the nanocomposites of MoS_2@CNT, MoS_2@Gr, and MoS_2@C60 could significantly reduce the COF of PAG base oil at HT, as well as improve the load carrying capacity of PAG at elevated temperatures, which might be attributed to the synergistic effect between MoS_2 and CNMs. However, C60 with a small surface area could not prevent MoS_2 NPs oxidation during rubbing, and the aggregation of MoS_2 NPs in MoS_2@C60 also weakened the synergistic effect, resulting in an inferior friction reduction and load carrying capacity of MoS_2@C60, as compared with MoS_2@CNT and MoS_2@Gr.

3.3 Surface analysis

The active elements on the worn surfaces lubricated by PAG and PAG along with various additives are investigated by SEM-EDS to explore the lubrication mechanism of MoS_2@CNT, MoS_2@Gr, and MoS_2@C60. The EDS spectra and element mapping images clearly showed the transfer/adsorption of molybdenum and

sulfur elements in the tribofilms formed on the worn surfaces lubricated by PAG containing MoS_2 NPs, MoS_2@CNT, MoS_2@Gr, and MoS_2@C60 (Figs. 8(e)–8(h)). However, molybdenum and sulfur elements are not detected on the worn surfaces lubricated by PAG and PAG added with CNT, Gr, and C60 (Figs. 8(a)–8(d)). These results indicated that molybdenum and sulfur elements are the predominant elements in the tribofilms from MoS_2 NPs, MoS_2@CNT, MoS_2@Gr, and MoS_2@C60, which attribute towards significantly improving the

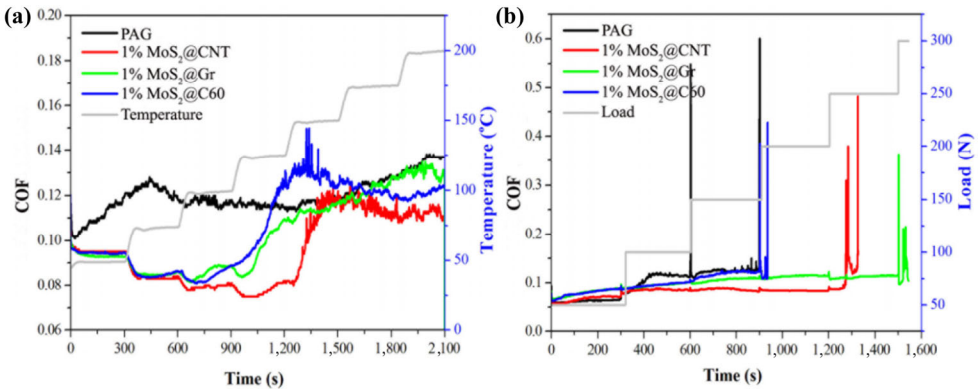

Fig. 7 COF of the steel discs lubricated by PAG base oil and PAG containing 1 wt% CNT, 1 wt% Gr, 1 wt% C60, 1 wt% MoS_2, 1 wt% MoS_2@CNT, 1 wt% MoS_2@Gr, and 1 wt% MoS_2@C60 at various (a) temperatures (load, 100 N; stroke, 1 mm; and frequency, 25 Hz) and (b) loads (temperature, 100 °C; stroke, 1 mm; and frequency, 25 Hz).

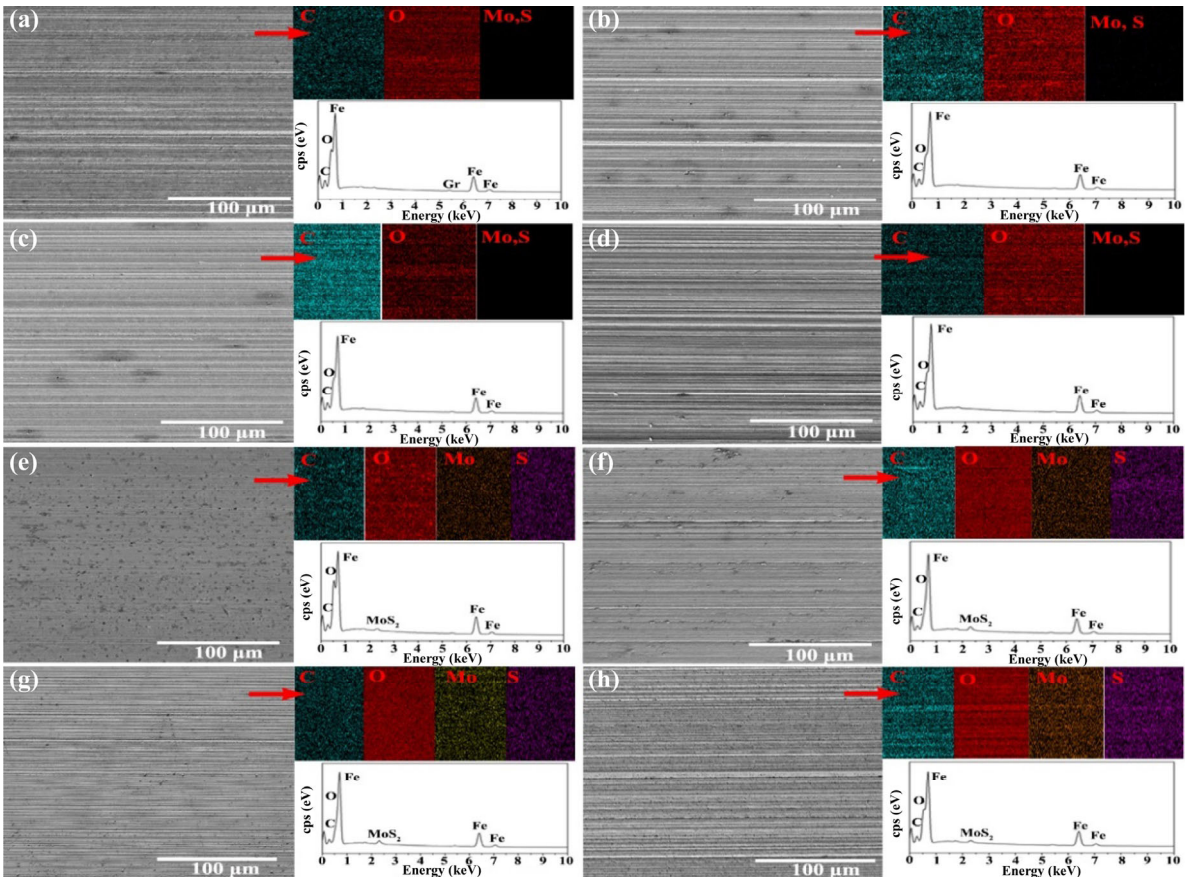

Fig. 8 Magnified SEM images of the worn surfaces lubricated with (a) PAG base oil, and PAG containing (b) 1 wt% CNT, (c) 1 wt% Gr, (d) 1 wt% C60, (e) 1 wt% MoS_2, (f) 1 wt% MoS_2@CNT, (g) 1 wt% MoS_2@Gr, and (h) 1 wt% MoS_2@C60 at 100 °C (SRV conditions: load, 100 N; stroke, 1 mm; frequency, 25 Hz; and duration, 30 min). The corresponding EDS spectra and element mapping are also shown in (a–h).

AW property of PAG base oil at HT.

The possible surface contaminants of wear scars lubricated by PAG added with MoS_2@CNTs, MoS_2@Gr, and MoS_2@C60 at elevated temperature are characterized by XPS to further explore the friction reduction and AW mechanism of these nanocomposites. As shown in Fig. 9, there is almost no difference in the Fe 2p, Mo 3d, and S 2p XPS spectra of the tribofilm formed from 1 wt% MoS_2@CNTs, 1 wt% MoS_2@Gr, and 1 wt% MoS_2@C60, which indicates that the three nanocomposites on the wear surfaces had similar tribochemical

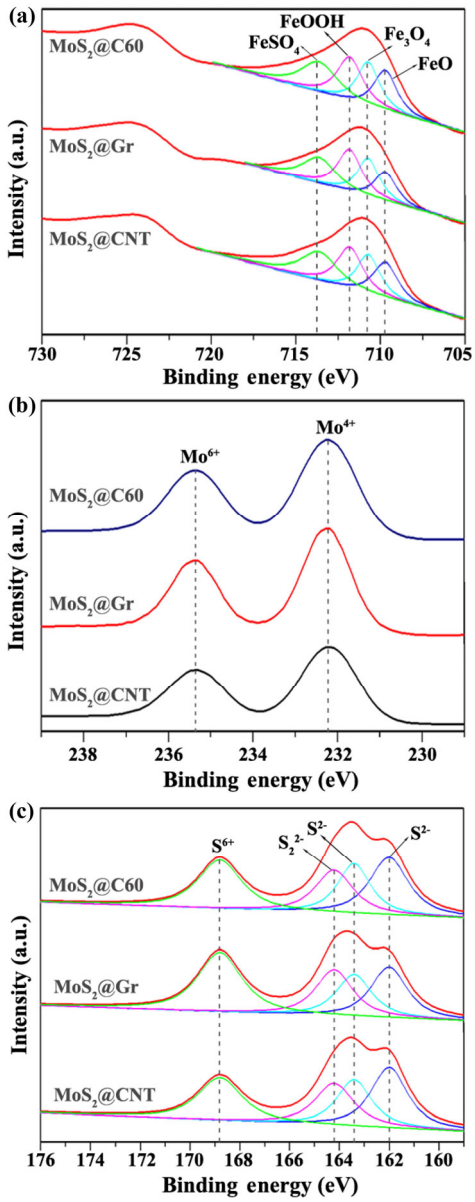

Fig. 9 (a) Fe 2p, (b) Mo 3d, and (c) S 2p XPS spectra of worn surfaces lubricated by PAG with 1 wt% MoS_2@CNT, MoS_2@Gr, and MoS_2@C60 at 100 °C and 100 N.

reactions during the sliding processes. Specifically, the high-resolution XPS spectra of Fe 2p can be deconvoluted into four peaks (Fig. 9(a)), and all the peaks at 709.6, 710.5, 711.6, and 713.5 eV actually correspond to FeO, Fe_2O_3, FeOOH, and $FeSO_4$, respectively [27]. The Mo 3d XPS spectra display two peaks (Fig. 9(b)), and one of those located at 232.4 eV is the characteristic of MoS_2 [20], while the other peak at higher binding energy (235.4 eV) corresponds to MoO_3 [27], which might be due to the oxidation of MoS_2 in those nanocomposites during the tribochemical reaction at HT in air. Furthermore, the XPS spectra of S 2p is composed of four peaks corresponding to MoS_2 (162.0 and 163.3 eV), S_2^{2-} (164.2 eV), and SO_4^{2-} (168.8 eV), respectively [20, 27]. The XPS result reveals that the addition of MoS_2@CNT, MoS_2@Gr, and MoS_2@C60 in PAG base oil might show similar tribochemical reactions on the rubbed surface to generate a complex protection film comprised of FeO, Fe_3O_4, FeOOH, $FeSO_4$, and MoS_2. The boundary lubrication film essentially contributes to the exceptional tribological performance of MoS_2@CNMs [28]. However, the MoS_2 will be easily oxidized to form MoO_3 under an elevated temperature, resulting in a lubrication failure under severe conditions. Benefitting from the synergistic effect between MoS_2 and CNMs [14], the addition of MoS_2@CNT, MoS_2@Gr, and MoS_2@C60 nanocomposites in PAG base oil exhibit superior anti-oxidation property and lubrication than the addition of MoS_2 NPs under HT condition.

4 Conclusions

The nanocomposites of MoS_2@CNT, MoS_2@Gr, and MoS_2@C60 were prepared by using a simple solvothermal method for use as potential HT lubricant additives. Their structures were characterized by different techniques, such as SEM, HRTEM, XPS, Raman spectra, and XRD. The result showed that MoS_2 with particle size ranging from 50 to 100 nm were uniformly grown on the surfaces of CNT, Gr, and C60. By benefitting from the synergistic effect between MoS_2 and CNMs, MoS_2@CNT, MoS_2@Gr, and MoS_2@C60 displayed superior oil dispersibility than the pure MoS_2 NPs, and significantly reduced the friction and wear of PAG compared to CNT, Gr, C60, and MoS_2 NPs at HT. They also improved the maximum load

carrying capacity of PAG from 100 to 250, 200, and 150 N, respectively. Furthermore, MoS_2@CNT and MoS_2@Gr had better friction reduction and load carrying capacity than MoS_2@C60, because C60 with small surface area could not prevent MoS_2 NPs oxidation during rubbing and the aggregation of MoS_2 NPs in MoS_2@C60 would weaken the synergistic effect. The excellent tribological behavior of MoS_2@CNT, MoS_2@Gr, and MoS_2@C60 was attributed to the formation of a boundary lubrication film composed of FeO, Fe_3O_4, FeOOH, $FeSO_4$, and MoS_2.

Acknowledgements

This work was financially supported by the National Key Research and Development Program of China (2018YFB2000601) and National Natural Science Foundation of China (Nos. 51875553 and 51775536).

References

[1] Mortier R M, Fox M F, Orszulik S T. *Chemistry and Technology of Lubricants*. Dordrecht: Springer, 2010.

[2] Trivedi H K, Forster N H, Saba C S. Rolling contact fatigue testing of a 3 cSt polyolester lubricant with and without TCP and DODPA/PANA at 177 °C. *Tribol Lett* **16**(3): 231–237 (2004)

[3] Neale M J. *The Tribology Handbook*. 2nd edn. Oxford: Butterworth-Heinemann, 1995.

[4] Masuko M, Hirose S, Okabe H. Boundary lubrication characteristics of polyol ester-class synthetic lubricants applied to silicon nitride at high temperature up to 280 °C. *Lubr Eng* **52**: 641–647 (1996)

[5] Rudnick L R, Shubkin R L. *Synthetic Lubricants and High-Performance Functional Fluids*. New York: Marcel Dekker, 1999.

[6] Çavdar B. Effect of temperature, substrate type, additive and humidity on the boundary lubrication in a linear perfluoropolyalkylether fluid. *Wear* **206**(1−2): 15−23 (1997)

[7] Gao X L, Liu D H, Song Z, Dai K. Isosteric design of friction-reduction and anti-wear lubricant additives with less sulfur content. *Friction* **6**(2): 164–182 (2018)

[8] Erdemir A, Ramirez G, Eryilmaz O L, Narayanan B, Liao Y F, Kamath G, Sankaranarayanan S K R S. Carbon-based tribofilms from lubricating oils. *Nature* **536**(7614): 67–71 (2016)

[9] Wright R A E, Wang K W, Qu J, Zhao B. Oil-soluble polymer brush grafted nanoparticles as effective lubricant additives for friction and wear reduction. *Angew Chem Int Ed* **55**(30): 8656–8660 (2016)

[10] Uflyand I E, Zhinzhilo V A, Burlakova V E. Metal-containing nanomaterials as lubricant additives: State-of-the-art and future development. *Friction* **7**(2): 93–116 (2019)

[11] Yu R, Liu J X, Zhou Y. Experimental study on tribological property of MoS_2 nanoparticle in castor oil. *J Tribol* **141**(10): 102001 (2019)

[12] Rabaso P, Ville F, Dassenoy F, Diaby M, Afanasiev P, Cavoret J, Vacher B, Le Mogne T. Boundary lubrication: Influence of the size and structure of inorganic fullerene-like MoS_2 nanoparticles on friction and wear reduction. *Wear* **320**: 161–178 (2014)

[13] Chen Z, Liu X W, Liu Y H, Gunsel S, Luo J B. Ultrathin MoS_2 nanosheets with superior extreme pressure property as boundary lubricants. *Sci Rep* **5**: 12869 (2015)

[14] Xu Y F, Peng Y B, Dearn K D, Zheng X J, Yao L L, Hu X G. Synergistic lubricating behaviors of graphene and MoS_2 dispersed in esterified bio-oil for steel/steel contact. *Wear* **342–343**: 297–309 (2015)

[15] Gong K L, Wu X H, Zhao G Q, Wang X B. Tribological properties of polymeric aryl phosphates grafted onto multi-walled carbon nanotubes as high-performances lubricant additive. *Tribol Int* **116**: 172–179 (2017).

[16] Mutyala K C, Wu Y A, Erdemir A, Sumant A V. Graphene-MoS_2 ensembles to reduce friction and wear in DLC-Steel contacts. *Carbon* **146**: 524–527 (2019)

[17] Li Y G, Wang H L, Xie L M, Liang Y Y, Hong G S, Dai H J. MoS_2 nanoparticles grown on graphene: An advanced catalyst for the hydrogen evolution reaction. *J Am Chem Soc* **133**(19): 7296–7299 (2011)

[18] Wu X H, Gong K L, Zhao G Q, Lou W J, Wang X B, Liu W M. MoS_2/WS_2 quantum dots as high-performance lubricant additive in polyalkylene glycol for steel/steel contact at elevated temperature. *Adv Mater Interfaces* **5**(1): 1700859 (2018)

[19] Zhao J, He Y Y, Wang Y F, Wang W, Yan L, Luo J B. An investigation on the tribological properties of multilayer graphene and MoS_2 nanosheets as additives used in hydraulic applications. *Tribol Int* **97**: 14–20 (2016)

[20] Zheng X L, Xu J B, Yan K Y, Wang H, Wang Z L, Yang S H. Space-confined growth of MoS_2 nanosheets within graphite: The layered hybrid of MoS_2 and graphene as an active catalyst for hydrogen evolution reaction. *Chem Mater* **26**(7): 2344−2353 (2014)

[21] Yang X L, Jia Q J, Duan F H, Hu B, Wang M H, He L H, Song Y P, Zhang Z H. Multiwall carbon nanotubes loaded with MoS_2 quantum dots and MXene quantum dots: Non–Pt bifunctional catalyst for the methanol oxidation and oxygen reduction reactions in alkaline solution. *Appl Surf Sci* **464**: 78–87 (2019)

[22] Ojeda-Aristizabal C, Santos E J G, Onishi S, Yan A M, Rasool H I, Kahn S, Lv Y C, Latzke D W, Velasco Jr J, Crommie M F, et al. Molecular arrangement and charge transfer in C_{60}/graphene heterostructures. *ACS Nano* **11**(5): 4686−4693 (2017)

[23] Xu S J, Li D, Wu P Y. One-pot, facile, and versatile synthesis of monolayer MoS_2/WS_2 quantum dots as bioimaging probes and efficient electrocatalysts for hydrogen evolution reaction. *Adv Funct Mater* **25**(7): 1127–1136 (2015)

[24] Štengl V, Henych J. Strongly luminescent monolayered MoS_2 prepared by effective ultrasound exfoliation. *Nanoscale* **5**(8): 3387–3394 (2013)

[25] Talyzin A, Jansson U. C_{60} and C_{70} solvates studied by Raman spectroscopy. *J Phys Chem B* **104**(21): 5064–5071 (2000)

[26] Koroteev V O, Bulushev D A, Chuvilin A L, Okotrub A V, Bulusheva L G. Nanometer-sized MoS_2 clusters on graphene flakes for catalytic formic acid decomposition. *ACS Catal* **4**(11): 3950−3956 (2014)

[27] NIST X-ray photoelectron spectroscopy database. http://srdata.nist.gov/xps/, 2012.

[28] Liu L C, Zhou M, Jin L, Li L C, Mo Y T, Su G S, Li X, Zhu H W, Tian Y. Recent advances in friction and lubrication of graphene and other 2D materials: Mechanisms and applications. *Friction* **7**(3): 199–216 (2019)

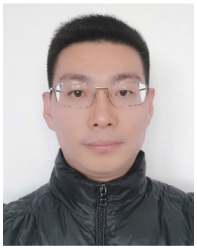

Kuiliang GONG. He earned his master's degree (2010) in materials science from Qingdao University in China. He is currently a Ph.D. candidate in Lanzhou Institute of Chemical Physics. His research focuses on nano-additives for lubricating oil.

Xiaobo WANG. He is a full professor in Lanzhou Institute of Chemical Physics (LICP), Chinese Academy of Sciences (CAS). He received his Ph.D. degree in physical chemistry from LICP in 2004. His research interest includes lubricating oils and greases, nano-additives, and tribochemical and tribophysical. He has published more than 150 peer reviewed journals papers and authorized 19 patents.

Xinhu WU. He got his Ph.D. degree in 2018 at Lanzhou Institute of Chemical Physics, CAS. He is an assistant at State Key Lab of Solid Lubrication in Lanzhou Institute of Chemical Physics, CAS. His research interests are HT lubricating oil and additives.